

Quantifying Chaos in Models of the Solar Neighbourhood

Dalia Chakrabarty¹ and Ioannis V. Sideris²

¹ School of Physics & Astronomy, University of Nottingham, Nottingham NG7 2RD, U.K. e-mail: dalia.chakrabarty@nottingham.ac.uk

² Institute for Theoretical Physics, University of Zürich, Winterthurerstrasse 190, Zürich CH-8057, Switzerland. e-mail: sideris@physik.unizh.ch

October 31, 2018

ABSTRACT

Aims. To quantify the amount of chaos that exists in the local phase space.

Methods. A sample of orbits from four different models of the Solar neighbourhood phase space are analysed by a new chaos identification (and quantification) technique. While three of the used models bear the signature of the perturbation due to both the Galactic bar and the spiral pattern, the last of the models is a bar only one. We explore the models by inter-comparing the corresponding values of chaos strength that is induced at the various energy levels.

Results. (1) We find that of all the viable models that have been demonstrated to successfully reproduce the local phase space structure, i.e. those that include the bar as well as the spiral, bear strong chaoticity, though the model that implies the highest degree of chaos is the one in which overlap of the major resonances of the bar and the spiral occurs. The bar only model is found to display regularity. (2) We advance chaos to be primarily responsible for the splitting of the Hyades-Pleiades mode (the larger mode) of the local velocity distribution

Key words. chaos – Galaxy – solar neighbourhood

1. Introduction

The availability of transverse velocities of nearby stars from *Hipparcos*, facilitated the construction of the local phase space distribution (Fux 2001; Skuljan et. al 1999; Dehnen 1998). In contradiction to the conventional idea of stellar dynamics, all representations of this distribution manifest strong non-linearity and multi-modalness. This clumpy nature of the solar neighbourhood velocity distribution (f) has been addressed in (Fux 2001; Quillen 2003; Dehnen 2000; Chakrabarty 2007; Famaey et. al 2005; de Simone et. al 2004) and others; consensus appears to be emerging as to the origin of the basic bimodal nature of the distribution in terms of scattering off the Outer Lindblad Resonance of the Galactic bar (OLR_b).

However, a dynamical basis for the existence of the other structure (such as the Hyades, Pleiades, Sirius, Coma Berenicus stellar streams) has attracted less of a focus. Chakrabarty (2007) (hereafter, Paper I) concluded the observed phase space structure to be due to the dynamical influence of the

Galactic bar and 4-armed spiral pattern; the influence of the bar alone, or the spiral alone were reported to be insufficient in explaining the present day observations of the solar neighbourhood. Quillen (2003) invoked the chaos caused by the overlapping of the OLR_b and the 4:1 resonance of the Galactic spiral pattern to explain the chaos dominated state of the local disk, a ramification of which, it was suggested, is the clumpy nature of f .

In spite of these investigations, the quantification of the degree of chaos in the solar vicinity, has not been undertaken yet. This is of interest in interpreting the state of the local patch in the disk and extrapolate this notion to the understanding of the Galactic disk as a whole as well as of outer disks in external spiral systems. The former of these motivations is to get a boost in the near future, with the quantity and spatial cover promised in the data from the upcoming *GAIA* mission. Here we present a new technique for estimating the amount of chaos that is induced in the solar neighbourhood, by the Galactic bar and spiral pattern. The different models used in Paper I will be analysed by the technique advanced in Sideris (2006). Thus, the aim of this paper is to evaluate the extent of chaos in the solar neighbourhood and ex-

Send offprint requests to: Dalia Chakrabarty

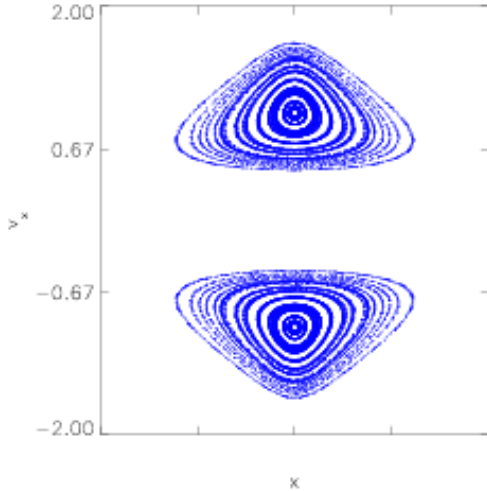


Fig. 1. Poincaré section for the bar-only model, at the energy of -0.75 . The white inner regions mark the part of $x - v_x$ space that is not populated by orbits for the specific implementation of our numerical experiment. The blue lines are invariant curves, (i.e. curves representing the 4-d regular orbits in the 2-dimensional Poincaré space).

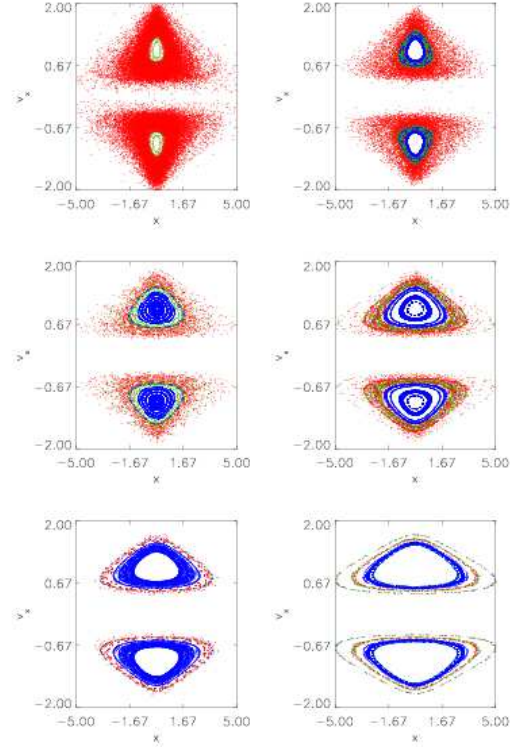


Fig. 2. Surface of sections of orbits integrated in the model with spiral to bar pattern speed ratio of $21/55$. Red signifies strong chaos, green signifies weak chaos and blue signifies regularity. Each panel represents a surface of section plot for a particular energy value; top left panel corresponds to $J=-0.300$, top right to -0.5 , middle left to -0.75 , middle right to -1.0 , bottom left to -1.25 and bottom right to orbits corresponding to energy of -1.5 . It is evident that chaos decreases as energy decreases.

amine the possible connection between the identified chaos and the local phase space structure.

This paper is organised as follows. The following section deals with the models, while in §3 the equations of motion are briefly discussed. The chaos quantification technique is advanced in §4 and the recovered results are presented herein. §5 is dedicated to a discussion of some aspects of the work. The paper is rounded off with the concluding remarks in §6.

2. Models of the Local Disk

As said before, here we endeavour to infer the degree of chaos present in the vicinity of the Sun by gauging chaoticity of solar neighbourhood models that were presented in Paper I. Thus, the justification of the choice of the relevant parameters will not be repeated here; rather, it is the aspect of quantification of the chaos inherent in each of these models that we discuss below.

In Paper I, an annulus in the outer part of the Galactic disk was modelled by test particle simulations, in which a warm exponential disk was stirred by the bar or a spiral pattern alone, or by both these perturbations jointly. In these simulations, the Galactic disk is assumed to be ideal with the disk stars assumed to be drawn from a 4-D phase space. A sample of phase space coordinates were chosen from a model initial phase space distribution function (chosen to ensure an exponential surface mass density profile and enough warmth to attain the velocity dispersions and vertex deviation observed in the

solar neighbourhood today). These coordinates were allowed to evolve with time in the presence of the potential of the disk and the perturbation(s), i.e. the bar or (and) spiral. The bar was modelled as a rigidly rotating quadrupole (see Equation 1 in Paper I) with a perturbation strength that is half the strength of the bar used in Fux, 2001. The spiral pattern is modelled as a logarithmic spiral that is 4-armed (Vallée 2002) and tightly wound (pitch angle of 15°), as the model spiral pattern used by Johnston et. al (2001); this choice of number of arms and a low pitch angle also ties in with the suggestion of Melnik (2006); Bissantz et. al (2003); Englmaier & Gerhard (1999); Vallée (2002). The initial disk configuration is characterised by a logarithmic potential to ensure flat rotation curve and a doubly-cut out distribution function (Evans & Read 1998) that ensures an exponential surface stellar mass density profile. This distribution function is parametrised by a hotness parameter that is maintained sufficiently high to ensure the re-

covery of velocity dispersions and vertex deviation that match with the observed values of these quantities in the solar neighbourhood today.

The orbits were recorded in the annulus between $R = 1.7R_{CR}$ to $R = 2.3R_{CR}$, where R_{CR} is the corotation radius of the bar; OLR_b occurs at $1.7R_{CR}$ for the above mentioned choice of the disk potential. In this work, all lengths are expressed in units of R_{CR} and given the scale free nature of our disk configuration, the physical value of R_{CR} is not relevant. An important parameter that was varied to define the individual models is the ratio between the pattern speeds of the bar (Ω_b) and the 4-armed spiral (Ω_s). In every other respect, the bar+spiral models are similar to each other. The bar-only model is similar to the bar+spiral models in every respect except that there is no perturbation from the spiral in this model. Likewise for the spiral-only model. Thus, the 5 models used in Paper I are:

- bar alone perturbing disk.
- bar and spiral acting in concert with $\Omega_b/\Omega_s=55/25$.
- bar and spiral acting in concert with $\Omega_b/\Omega_s=55/21$.
- bar and spiral acting in concert with $\Omega_b/\Omega_s=55/18$.
- spiral acting alone.

From Paper I we learn that out of these 5 models, the first four were found to give rise to phase space structure that is reminiscent of the observed structure (checked via a hypothesis testing technique), though the bar-only model was rejected on further dynamical grounds. In particular, the bar+spiral model that is characterised by $\Omega_b/\Omega_s=55/21$ is the one that ensures that the ILR of the spiral (ILR_s) occurs at the same physical location as the OLR_b . Thus, this is the model that corresponds to overlap of the major resonances of the two perturbations therefore augers interesting dynamical consequences.

3. Equations of Motion

In this section, the stellar equations of motion are discussed. Below is presented the Hamiltonian in an inertial frame, in galactocentric coordinates x_i , for $i=1,2$ and their conjugate momentum (or velocity v_i), given the logarithmic potential of the background disk ($\sim \ln(R)$, where $R = \sqrt{x_1^2 + x_2^2}$) and the perturbations due to the quadrupolar bar (Φ_{bar}) and the logarithmic $m=4$ spiral pattern (Φ_{spiral}).

$$\mathcal{H} = \sum_1^2 v_i^2 + \ln(R) + \Phi_{bar} + \Phi_{spiral}, \quad (1)$$

where the potential of the bar and the spiral in our scale-free units (i.e., all lengths are expressed in units

of the bar corotation radius), in the inertial frame, at time t are:

$$\Phi_{bar} = -\epsilon_{bar} \frac{\cos 2(\phi - \Omega_b t)}{R^3}$$

$$\Phi_{spiral} = -\epsilon_{spiral} K(\alpha, m) e^{i[m(\phi - \Omega_s t)]} R^{i\alpha - \frac{1}{2}}. \quad (2)$$

Here $\alpha = m \cot(i)$, where i is the pitch angle of the spiral and m is the number of arms in the pattern ($i=15^\circ$ and $m=4$ for our models). $K(\alpha, m)$ is the Kalnajs gravity function as defined in Equation 13 of Chakrabarty (2004). Also, ϵ_{bar} and ϵ_{spiral} are the bar and spiral strengths, defined in terms of the fractional contribution of the particular perturbation to the field due to the background disk ($\approx 3.6\%$ for the bar and the spiral). Lastly, here ϕ is the azimuthal coordinate: $\phi = \tan^{-1}(x_2/x_1)$. See Section 2.2 of Chakrabarty (2004) for a detailed discussion of the equations of motion.

Thus, in the inertial frame, the equations of motion are:

$$\ddot{\mathbf{x}}_i = \frac{-\mathbf{x}_i}{R^2} - \nabla \Phi_{bar} - \nabla \Phi_{spiral}. \quad (3)$$

When the only imposed perturbation is the bar, recording the orbits in the frame of the bar implies that the Jacobi Integral is:

$$\mathcal{H}_J = \sum_1^2 v_i^2 + \ln(R) - \epsilon_{bar} \frac{\cos 2\phi}{R^3}. \quad (4)$$

Thus, in this case, \mathcal{H}_J is an integral of motion and the surfaces of section that are recovered for this 4-D phase space, by setting $v_y=0$, is two dimensional.

However, in the multiple pattern speed scenario, the Hamiltonian is no longer the Jacobi Integral; thus, when the spiral pattern is included as the second perturbation, and the orbits recorded in the frame rotating with the bar, the orbital energy is:

$$\mathcal{H}_J = \sum_1^2 v_i^2 + \ln(R) - \epsilon_{bar} \frac{\cos 2(\phi)}{R^3} - \epsilon_{spiral} K(\alpha, m) e^{i[m(\phi - (\Omega_s - \Omega_b)t)]} R^{i\alpha - \frac{1}{2}}. \quad (5)$$

It is obvious that the quantity \mathcal{H}_J in Equation 5 returns to the same value periodically for period $T = m * \pi / (\Omega_b - \Omega_s)$, so if data are recorded stroboscopically every such period, \mathcal{H}_J is equivalent to an integral of motion. Then out of the recorded points per orbit (which are recorded only when $t = T$) one can construct two-dimensional surfaces of section by employing a second constraint, in our case by choosing to plot only the points which have $v_y=0$. Any other constraint one may impose, e.g. $v_x=0$, should give the same results regarding the percentages of chaotic and regular orbits or strengths of chaos, since we quantify the same set of orbits but at a different surface section.

4. Quantification of Chaos and Results

The quantification of chaos for the orbits of this paper was achieved by the use of a new measure first introduced by Sideris (2006). This technique is based on the recognition of smooth patterns in the signals associated with an orbit. It was shown in the original paper that the extrema of regular orbits correlate in such ways so to build smooth curves. This inherent smoothness, typically hidden inside the signal, can then be implemented to define a measure of regularity, through an intricate interpolation scheme. The simple picture is that the smoother the curves the more regular the signal is.

A chaotic orbit usually evolves in a divided phase space (a phase space which is characterised by both regular and chaotic regions Contopoulos (2002); Sideris (2008)). In such a regime, any chaotic orbit (provided it is integrated for long enough timescales) will experience two kinds of dynamical epochs: strong or wild chaos and weak or sticky chaos Shirts & Reinhardt (1982); Contopoulos (2002). Strong chaos is associated with motion of the orbit far away from the regular islands. Such motion is completely unpredictable, and the chaotic orbit attempts to cover broad parts of the chaotic sea energetically available to it. When the orbit moves close to the regular islands it becomes trapped for a long time around them, in practice, attempts to mimic regularity. The closer to a regular island the chaotic orbit moves the more persuasive this mimicry is.

The patterns method can identify when an orbit gets into weakly chaotic regimes. Semi-smooth curves correlating extrema of the signal of the orbit appear in that epoch of its evolution. The big advantage of the pattern method is that it treats orbits as sets of segments, piece by piece, and not as one monolithic entity as other measures typically do. This is how it achieves to distinguish parts of the orbit where weak chaos is experienced.

We applied this method to the orbits associated with the aforementioned simulations. For every simulation a number of orbits that correspond to a given value of energy, were randomly extracted in several different energy bands and the chaos quantification followed.

For the bar only model for the six energies evolved (from -0.3 to -1.5) no chaos was found. In Figure 1, we show a surface of section that is constructed for orbits characterised by an energy of -0.75. All the surfaces of sections presented herein are recorded for the orbits crossing the plane $v_y = 0$.

The results for six different energies for the ratio 21/55 can be seen in Figure 2. Similar pictures hold true for models 18/55 and 25/55. In all three models it is obvious that chaos is very strong for large energies but reduces as energy decreases.

To compare the chaos inducing ability of the different models, the fraction of the regular and

(strongly and weakly) chaotic orbits is shown in Figure 3. These plots show the percentage of chaotic orbits appearing in the three models. One may notice that the case 21/55 is quantified as more chaotic than the other cases.

In Figure 4 the chaos strength is plotted with respect to the energy for the four models $\Omega_s/\Omega_b=18/55, 21/55, 25/55$ and the bar-only.

5. Discussions

Our chaos quantification technique helps shed light on the models; we find that at the higher energies, *the model that manifests the highest chaos is the model that ensures resonance overlap* (the 21/55 model). This is in line with our expectations of course, but it is also interesting to note that the *chaos induced by the other bar+spiral models is not much less either*. At the same time, from Paper I, we know that all three of the bar+spiral models were successful in explaining the observed structure of the local phase space. This adds weight to the suggestion that *chaos is responsible for the clumps of the local velocity space*. (Of course, this is only part of the story, since scattering off the Outer Lindblad Resonance of the bar and the effects of minor resonances of the bar and the spiral are also important, as reported in Paper I).

To understand the trends in our results, we need to invoke the following: the ILR of the spiral pattern is an "angular momentum emitter" (Lynden-Bell & Kalnajs 1972), the basic effect of which is to "stir without heating" (Sellwood & Binney 2002). This idea that the Inner Lindblad Resonance of the spiral (ILR_s) is the location from which stars are driven outwards, is corroborated by the experiments of Chakrabarty (2004). Now in our modelling, we choose to record our orbits in an annulus that extends from $R = 1.7R_{CR}$ to $2.3R_{CR}$, where R_{CR} is the corotation radius of the bar. So the occurrence of ILR_s at $R < 1.7R_{CR}$ (the 25/55 model) implies that stars will be pushed into the relevant annulus from lower radii than when ILR_s concurs with the physical location of OLR_b . In the case ILR_s occurs at $1.7R_{CR} < R < 2.3R_{CR}$, (the 18/55 model), a part of the annulus will be depleted at the cost of the parts at radii around $2.3R_{CR}$. Thus, for the 25/55 model, more stars will be entering our annulus from lower energies than in the other two models. Now, in a smooth unperturbed background potential, stars at lower radii are also more energetic than those at higher radii. This implies that in the absence of resonances due to imposed perturbations, there would have been more high energy stars recorded for the 25/55 case than in the 18/55 or 21/55 models.

This situation is of course challenged once the perturbations are introduced - in particular, proximity to resonance overlap indicates enhanced chaoticity in the recorded orbits. The relative excess in the energy

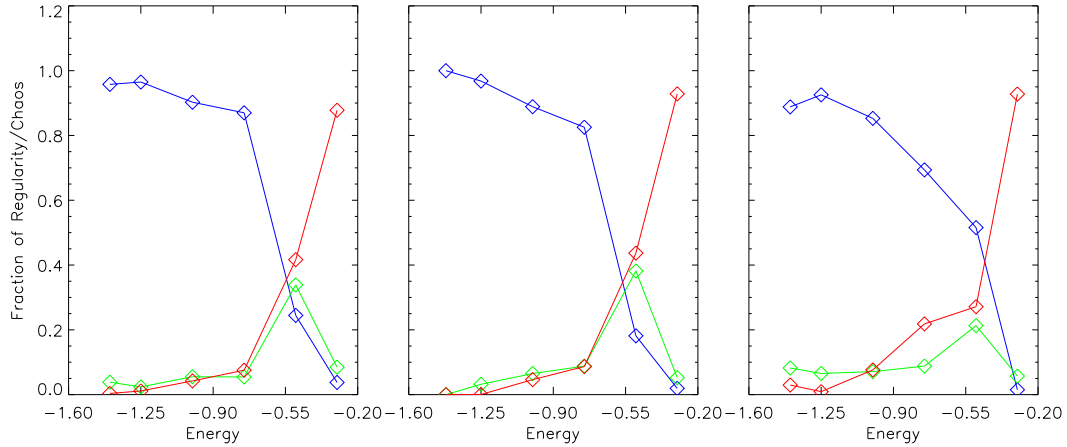


Fig. 3. Fractions of chaotic orbits (in red), weakly chaotic orbits (in green) and regular orbits (in blue), plotted as functions of energy, for the three bar+spiral models 18/55 (left), 21/55 (middle), 25/55 (right).

of the recorded orbits, as implied by the 25/55 model is surpassed, more at higher energies than lower, by the strength of chaos that is a signature of the resonance overlap case. This explains the relative trends in chaos strength that is noticed in the different models (Figure 4).

We conclude that the observed phase space structure in the Solar neighbourhood (particularly the splitting of the Hyades-Pleiades mode) is to a large extent, chaos induced. But this chaos does not necessarily have to be triggered by resonance overlap (in contradiction to what Quillen, 2003 suggested). In fact, the presence of *chaos is found to be actuated by the spiral potential*. We say this since our results indicate that the *bar potential alone is insufficient in producing chaos*. This is in contradiction to the suggestion by Fux (2001). The bar that was used in the modelling in Paper I (our models) imposes a field of 3.6% of that of the background disk, nearly half of what was used by Fux (2001). Thus, it may be argued that it is this low a bar strength that was incapable of heating the disk enough; after all, as shown in Chakrabarty (2004), disk heating increases rapidly with increases in bar strength.

6. Conclusions

In this work, we have presented a neat way of quantifying chaos that shows up in models of the local phase space. This work needs to be buttressed in the future with more sophisticated models that span all six phase space dimensions and account for the Galactic halo as well. This objective estimation and classification of orbits into strongly chaotic, weakly chaotic and regular, allows us to understand the local phase space in greater details than has been possible before. We implement this technique on models of the Solar neighbourhood to conclude that all

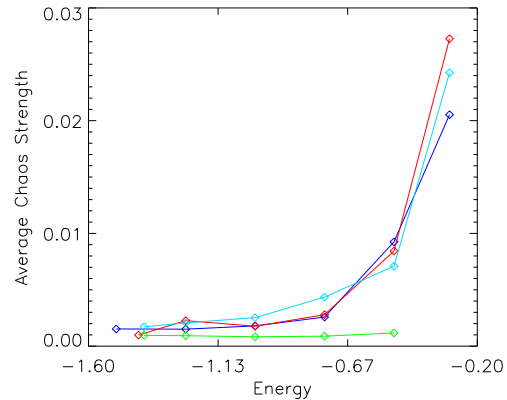


Fig. 4. Average strength of chaos against energy, for the four models 18/55, 21/55, 25/55 and bar only. Blue signifies the 18/55 model, red 21/55, cyan 25/55 and green the bar only model.

models that include the spiral pattern exhibit chaoticity and this nature of the local phase space is advanced as an important contributor to the formation of the observed phase space structure. We advance this technique as a blueprint for evaluating the degree of chaos present in kinematic samples that would be collated in the near future by GAIA.

Acknowledgements. DC is supported by a Royal Society Dorothy Hodgkin Fellowship. IVS is supported by the Tomalla Foundation.

References

- Bissantz, N. and Englmaier, P. and Gerhard, O., 2003, MNRAS, 340, 949.
- Chakrabarty, D., 2007, A&A, 467, 145.
- Chakrabarty D., 2004, MNRAS, 352, 427.

- Contopoulos G., Order and Chaos in Dynamical Astronomy, Springer-Verlag, Berlin (2002).
- Dehnen, W., 2000, AJ, 119, 800.
- Dehnen, W., 1998, AJ, 115, 2384.
- De Simone, R., Wu, X. and Tremaine, S., 2004, MNRAS, 350, 627.
- Englmaier, P., & Gerhard, O. 1999, MNRAS, 304, 512
- Evans, N. W. and Read, J. C. A., 1998, MNRAS, 300, 83.
- Famaey, B., Jorissen, A., Luri, X., Mayor, M., Udry, S., Dejonghe, H. and Turon, C., 2005, *Å*, 430, 165.
- Fux, R., 2001, AJ, 373, 511.
- Johnston, S., Koribalski, B., Weisberg, J. M. and Wilson, W., 2001, MNRAS, 322, 715.
- Lynden-Bell, D. and Kalnajs, A., 1972, 157, 1.
- Melnik, A., 2006, *Astron. Lett.*, 32, 7.
- Quillen, A. C., 2003, AJ, 125, 785.
- Sellwood, J. A., & Binney, J. J., 2002, MNRAS, 336, 785
- Shirts, R. B. & Reinhardt, W. P., 1982, J. Chem. Phys. 77, 5204.
- Sideris, I. V., 2006, Phys. Rev. E, 73, 066217.
- Sideris, I. V., Phys. Rev. E, submitted.
- Skuljan, J., Hearnshaw, J. B. and Cottrell, P. L., 1999, MNRAS, 308, 731.
- Vallée, J. P., 2002, ApJ, 566, 261.